IOP Publishing Mater. Quantum Technol. 5 (2025) 023002 https://doi.org/10.1088/2633-4356/add830

Materials for Quantum Technology

OPEN ACCESS

RECEIVED
1 April 2025

REVISED
27 April 2025

ACCEPTED FOR PUBLICATION
13 May 2025

PUBLISHED
22 May 2025

PERSPECTIVE

Integrating quantum materials into superconducting qubits

Kuei-Lin Chiu[1,*], Avishma J Lasrado[1], Cheng-Han Lo[1], Chung-Ting Ke[2], Vahid Mosallanejad[3] and Yen-Hsiang Lin[4]

[1] Department of Physics, National Sun Yat-Sen University, Kaohsiung 80424, Taiwan
[2] Institute of Physics, Academia Sinica, Taipei 115201, Taiwan
[3] Institute of Natural Sciences, Westlake Institute for Advanced Study, Hangzhou, Zhejiang 310024, People's Republic of China
[4] Department of physics, National Tsing-Hua University, Hsinchu 300044, Taiwan
[*] Author to whom any correspondence should be addressed.

E-mail: klc@mail.nsysu.edu.tw

Keywords: superconducting qubits, quantum materials, 2D materials, quantum computing

Abstract

In this perspective article, we review the current state of research on integrating quantum materials (QMs) into superconducting quantum devices. We begin with the role of QMs as weak links in Josephson junctions, enabling gate- and flux-tunable transmons. We then explore their application in more complex superconducting circuits, such as gate-tunable fluxonium qubits, or gatemonium, which provide additional control over qubit parameters. We also discuss QM-based vertical junctions and their potential for creating merged-element transmons. Further, we highlight QMs' role in topological superconducting circuits, where they facilitate the study of Majorana zero modes through signatures such as 4π-periodic supercurrents. Additionally, we review the integration of QMs into 3D cavity architectures and discuss how they differ from their 2D counterparts. Beyond weak links, we examine the use of 2D superconducting and insulating materials, such as $NbSe_2$ and hBN, in parallel-plate capacitors, offering a compact alternative to conventional large-footprint transmon capacitors. Finally, we outline the current challenges and future directions for exploration.

1. Introduction

Quantum materials (QMs), owing to their rich internal degrees of freedom unexplored, provide versatile functions to be explored in quantum information science [1–5]. In particular, when QMs are reduced to low dimensions (1D or 2D), their physical properties can be significantly different from those of their bulk counterparts. An example of such is 1 T'-phase WTe_2, which is a Weyl semimetal in bulk but a 2D quantum spin Hall insulator in monolayer form [6, 7]. In addition, the interplay between stacked van der Waals (vdW) 2D materials generates novel physics such as the unconventional superconductivity discovered in twisted bilayer graphene and WSe_2 [8, 9]. On the other hand, Josephson junctions (JJs) are the key components in current state-of-the-art superconducting qubit devices [10, 11]. QM-based JJs reveal exotic physics, such as the possible Majorana zero modes (MZMs), reflected in the zero-bias peak, and a 4π-periodic supercurrent [12–19]. QMs in reduced dimensions can be used as a weak link in JJs for integration into superconducting qubits [20–27]. Similar to conventional Al/Al_2O_3 junctions, lateral JJs of QMs have been demonstrated as single-JJ transmons [28], as well as flux-tunable transmons using QM-based superconducting quantum interference devices (SQUIDs) [26, 29, 30]. Due to their reduced dimensions and gate tunable natures, QMs have also been demonstrated to form gate tunable transmons generally referred to as gatemons [21, 22, 25–27, 31, 32]. Gatemons have the capability of tuning the qubit frequency by electrostatic gate voltage, allowing another degree of freedom to access to different regimes in flux-tunable devices [33, 34]. On top of Josephson weak links, QMs such as $NbSe_2$ can be used as superconductors while hBN as dielectric layers in parallel-plate capacitors (PPCs) in conventional transmon devices [35, 36]. In an effort to evaluate the status of QMs for superconducting quantum technologies, we review recent research on utilizing QMs as various components in superconducting qubits. We begin with gate-tunable and flux-tunable transmon devices,

where QMs serve as weak links in JJs. We then extend our discussion to a more complex structure, the gate-tunable fluxonium, referred to as gatemonium. Subsequently, we address devices that incorporate vertical junctions and topological materials as weak links in transmon qubits. Next, we introduce studies on the integration of QMs with three-dimensional (3D) cavities, as well as their incorporation into other components of conventional Al/Al_2O_3-based superconducting qubits. Finally, we outline current challenges and potential future directions for exploration.

2. QMs serving as weak links in superconducting qubits

2.1. Gate-tunable and flux-tunable transmons

Unlike S-I-S (S stands for superconductor and I stands for insulator) junctions where the critical current is generally fixed after fabrications, the weak link in S-N-S (N stands for semiconductor or normal metal) junctions allows its carrier density to be tuned by gate voltage [2, 37]. Owing to the 1D, 2D natures and gate-tunable critical current, InAs nanowires (figure 1(a)), two-dimensional electron gas (2DEG, figure 1(b)) and graphene (figure 1(c)) can be used as a weak link in S–N–S junction-based gatemons [20–25, 29]. The first gatemon was realized in InAs nanowire, featuring a coherence time $T_1 \approx 0.8\ \mu$s and $T_2 \approx 1\ \mu$s, respectively [25]. Later, the coherence times $T_1 \approx 1.1\ \mu$s and $T_{2,\mathrm{echo}} \approx 2.2\ \mu$s were reported in 2DEG gatemons [22] while $T_1 \approx 36$ ns and $T_2^* \approx 51$ ns were observed in graphene gatemons [21]. All the studies above have demonstrated coherent controls of qubits, such as Rabi oscillations and Ramsey patterns. To further study the impact of flux noises and charge noises on the coherence properties, flux-tunable transmons [26, 29] and gate- and flux-tunable transmons [38] based on InAs nanowires were reported, as shown in figures 1(d) and (e), respectively. While the early study presented no correlation between the qubit coherence (based on qubit linewidth reduction) and charge sweet spot ($\partial f_{01}/\partial V_g = 0$) [26], the study in [29] presented elevated dephasing time $T_2 \approx 15\ \mu$s (similar to T_1) at the charge sweet spots, and concluded that on-chip charge noise dominates over electrical noise on the gate. In addition, this study also showed an enhanced T_2 ($\approx 30\ \mu$s) approaching $2T_1$ at the flux sweet spots ($\partial f_{01}/\partial \Phi = 0$) [29]. In [38], they presented a two-gatemon SQUID, allowing both the voltage and flux control of the potential profile in Hamiltonian, and the access to different qubit operation regimes corresponding to transmons or flux qubits. In the end, they demonstrated a relaxation time $T_1 \approx 7.2\ \mu$s resulting from an indirect transition between $|0>$ and $|1>$ in a so-called protected regime [38].

2.2. Gate-tunable fluxonium

Fluxonium qubits, since the first invention in 2009 [39], have become a promising research field for achieving long coherence times in superconducting qubits [40–42]. The heavy fluxonium with suppressed dipole matrix elements when biased to near half a flux quantum have reached a relaxation time $T_1 \approx 8$ ms [40], while 2D and 3D fluxoniums have both reported coherence times around 1 ms [41, 42]. Consequently, the integration of gate-tunable QM weak links in fluxonium qubits, enabling additional gate control, is of significant interest. InAs nanowire (figures 2(a)–(d)) and InAs 2DEG (figures 2(e)–(g)) weak links have been studied in gate-tunable fluxonium devices, which are generally referred as gatemonium [33, 34]. The first InAs nanowire gatemonium utilize a 50 nm-wide (Nb,Ti)N meander as a superinductor, which allows the application of large magnetic fields up to 1 Tesla [33]. Since large magnetic fields are required to access MZMs in semiconductor nanowire devices, this enables the potential use of the fluxonium as a readout device for topological qubits [33]. While coherent control has not been demonstrated in the InAs nanowire gatemonium, the second gatemonium using InAs 2DEG weak link and JJ array (superinductor) has successfully demonstrated Rabi oscillations in the plasmon regime and coherence times $T_1 \approx 78$ ns and $T_2 \approx 102$ ns [34]. Owing to the gate-tunable weak link, the Josephson energy E_J—and consequently the ratio between E_J and the charging energy E_C—is tunable via voltage. This enables smooth tuning between heavy and light fluxonium states (figure 2(h)), potentially allowing users to optimize either bit-flip or phase-flip times as needed [34]. Additionally, since the JJ array is also composed of InAs 2DEGs, it is possible to introduce gate tunability to the inductive energy E_L, providing further control over the gatemonium [34].

2.3. Vertical weak links

Most previously introduced QM-based circuit quantum electrodynamics (c-QED) devices have utilized lateral junctions as the weak links. However, vertical junctions using semiconductor tunnel barriers have also been integrated into single-junction transmons [43] and flux-tunable transmons [44]. Unlike the commonly used insulator Al_2O_3 in conventional superconducting qubits, which requires extremely thin barriers due to its large bandgap, semiconductor weak links have smaller bandgaps, allowing for thicker barriers that are less susceptible to pinhole formation compared to insulating barriers [44, 45]. This enables larger-area JJs with built-in capacitance, creating a more compact 'merged-element' transmon (MET) [46] without the need for

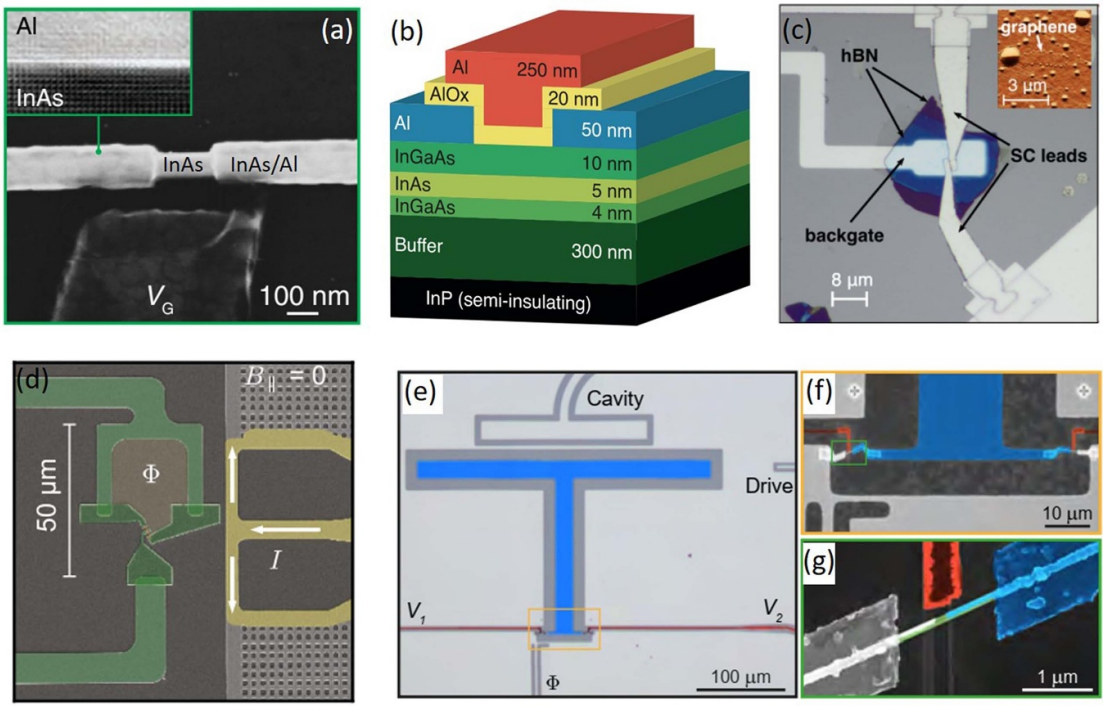

Figure 1. (a) InAs nanowire gatemon. Reprinted figure with permission from [25], Copyright (2015) by the American Physical Society. (b) InGaAs/InAs two-dimensional electron gas (2DEG) gatemon. Reproduced from [22], with permission from Springer Nature. (c) Graphene gatemon. Reproduced from [21], with permission from Springer Nature. (d) A flux-tunable InAs nanowire transmon. Reprinted figure with permission from [29], Copyright (2018) by the American Physical Society. (e)–(g) A flux- and gate-tunable InAs nanowire transmon consisting of two gate-tunable JJs. (f) False-color electron micrographs of the nanowire junctions. (g) A nearby electrostatic gate (red) allows for the tuning of the electron density in the junction. (e)–(g) Reprinted figure with permission from [38], Copyright (2020) by the American Physical Society.

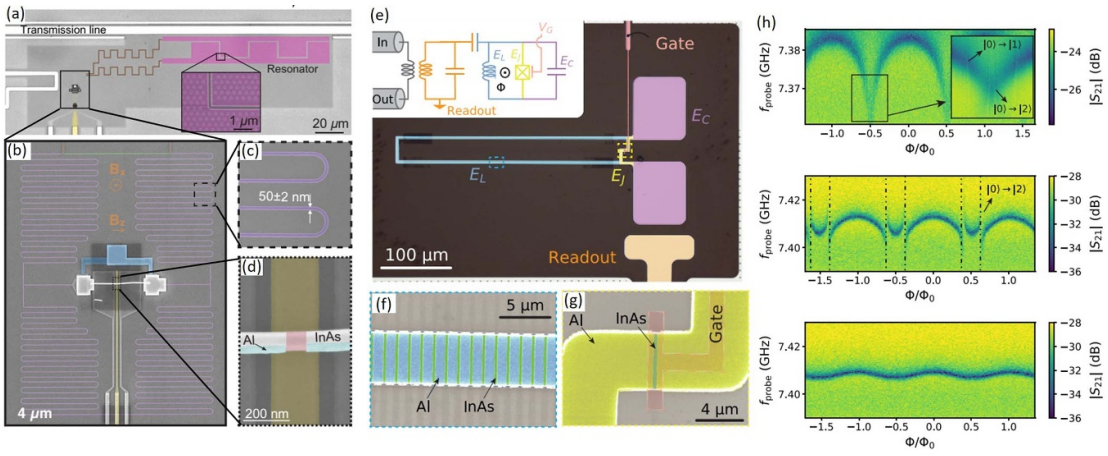

Figure 2. (a)–(d) Gate-tunable nanowire fluxonium. (a) False-colored optical image showing the transmission line and the resonator, with capacitive and inductive elements shaded in pink and brown, respectively. Inset: Scanning electron microscope (SEM) image of the resonator's capacitive plates. (b) SEM image of the area indicated by the box in (a). The (Nb,Ti)N superinductor [purple, enlarged in (c)], the shared inductance section (green), the parallel plate capacitor (blue), and the nanowire junction [red, enlarged in (d)]. Reprinted figure with permission from [33], Copyright (2020) by the American Physical Society. (e)–(g) Gate-tunable InAs 2DEG fluxonium. (e) A false-colored optical image of the device, consisting of a shunt capacitor (purple), a planar JJ (yellow), and a linear inductance, implemented in the form of a series of planar JJs (blue). The inset shows an equivalent-circuit diagram. (f) An enlarged SEM image of the JJ array. (g) A SEM image of the single junction before gate deposition. (h) The resonator spectroscopy of device transmission across the feedline (S21) is shown as a function of the applied external magnetic flux at different gate voltages (top: heavy regime, middle: intermediate regime, bottom: light regime). (e)–(h) Reprinted figure with permission from [34], Copyright (2025) by the American Physical Society.

large capacitor islands used in current superconducting qubits—an advantage for scalability. In the top panel of figure 3(a), a transmon consisting of a vertical Al/4 L-MoS_2/Al single JJ and a capacitor (which also serves as an antenna) is coupled to microwave photons within an aluminum 3D cavity [43]. The bottom panel of figure 3(a) shows the power dependent dispersive shift of the cavity's response. In this device, two-tone

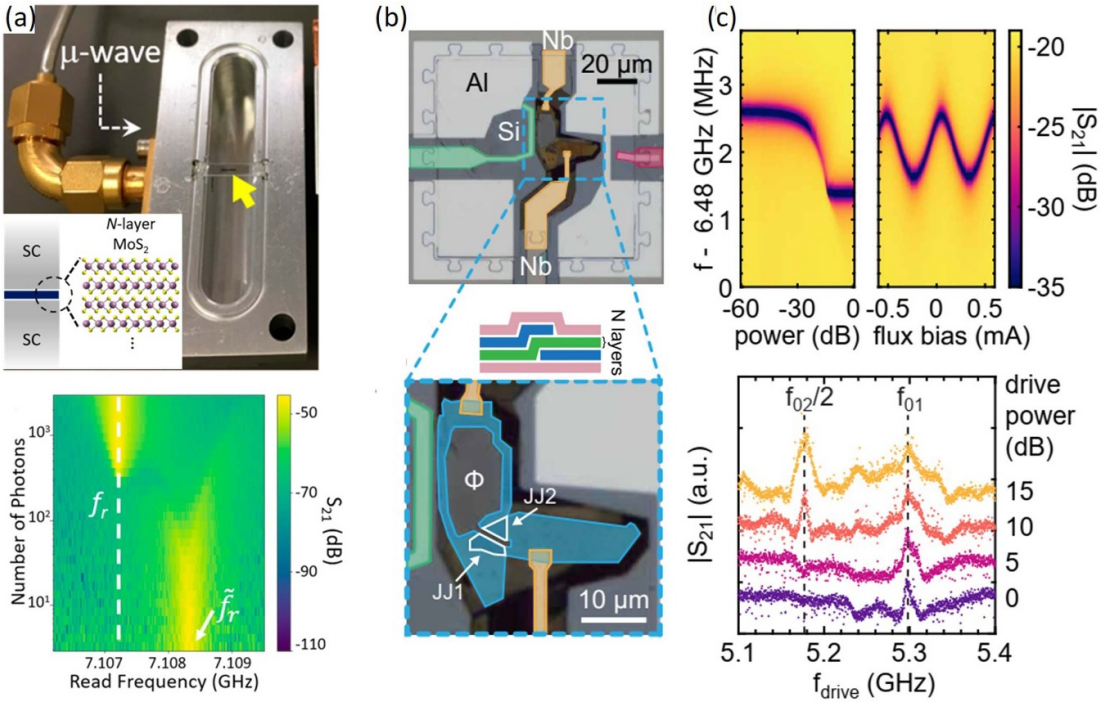

Figure 3. (a) Top panel: transmon based on MoS_2 vertical JJ coupled to a 3D cavity. The inset illustrates the JJ structure. Bottom panel: power dependence of cavity's response. Reprinted with permission from [43]. Copyright (2019) American Chemical Society. (b) Flux-tunable transmon based on $NbSe_2/WSe_2/NbSe_2$ vertical JJs. The inset shows the JJ structure, with hBN denoted by pink, $NbSe_2$ denoted by blue and WSe_2 denoted by green. (c) Data from the device shown in (b). Top panel: single-tone spectroscopy as a function of readout power (left) and flux bias current at low microwave power (right). Bottom panel: two-tone spectroscopy. Drive pulse power increases from purple to violet to pink to gold traces, which are vertically offset for clarity. (b) and (c) Reproduced from [44]. CC BY 4.0.

measurements have shown a qubit state transition, from which a coherence time $T_2^* \approx 12$ ns is estimated. The short coherence time was attributed to several factors: the large number of parasitic two-level systems due to the large junction size ($2 \times 2\,\mu m^2$), polymer residues potentially degrading junction quality, and dielectric loss in MoS_2. [43]. Figure 3(b) shows the all-vdW-material flux-tunable MET, comprising an $NbSe_2$/17-layer-thick $WSe_2/NbSe_2$ SQUID, which is capacitively coupled to the 2D coplanar readout resonator at one end, and to ground at the other end [44]. In this study, power dependence and flux-tuning of resonator's response were demonstrated, as well as the qubit state transition in two-tone measurements, as shown in the top and bottom panels of figure 3(c). However, the coherence properties of this qubit were not reported. Nevertheless, this study features an all crystalline merged-element transmon qubit, with the transmon frequency and anharmonicity closely matching the design parameters estimated from the thickness of the semiconductor tunnel barriers [44].

2.4. Topological materials

MZMs are a unique type of quasiparticle in condensed matter systems that obey non-Abelian exchange statistics and serve as key components for realizing topological quantum computing [47]. In 2008, Fu and Kane predicted that in a JJ consisting of 2D topological insulator (TI) edge states and s-wave superconductor (figure 4(a)), the Andreev Bound states (ABSs) would exhibit an exotic 4π-periodic modulation with magnetic flux, as shown in figure 4(b), rather than the conventional 2π-periodic one, serving as a signature of the existence of MZMs [48, 49]. Subsequently, the absence of the $n = 1$ Shapiro step, as evidence of the 4π-periodic supercurrent, has been observed not only in 2D TI systems (figure 4(c)) [15, 16] but also in other JJs composed of topological materials with helical bulk and edge states (figure 4(d)) [17, 18]. Alongside the fundamental interest in detecting MZMs, it is also intriguing to explore whether robust topological weak links could potentially serve as superconducting qubits [50, 51]. In particular, a transmon composed of a topological SQUID inherits the 4π-periodic nature of its constituent JJs and is therefore expected to exhibit a 4π-periodic qubit frequency under flux modulation (figure 4(e)) [52]. So far, integration of topological materials as a weak link in transmon architectures has been reported in Weyl semimetals [51] and TI nanostructures [28, 30]. Figure 5(a) shows a $MoTe_2$ SQUID coupled to a 2D coplanar readout resonator [51]. While flux modulation of resonator frequency was demonstrated, neither Rabi splitting nor qubit transitions were detected, suggesting a short coherence time [51]. Figure 5(b) illustrates a single-JJ transmon made of a

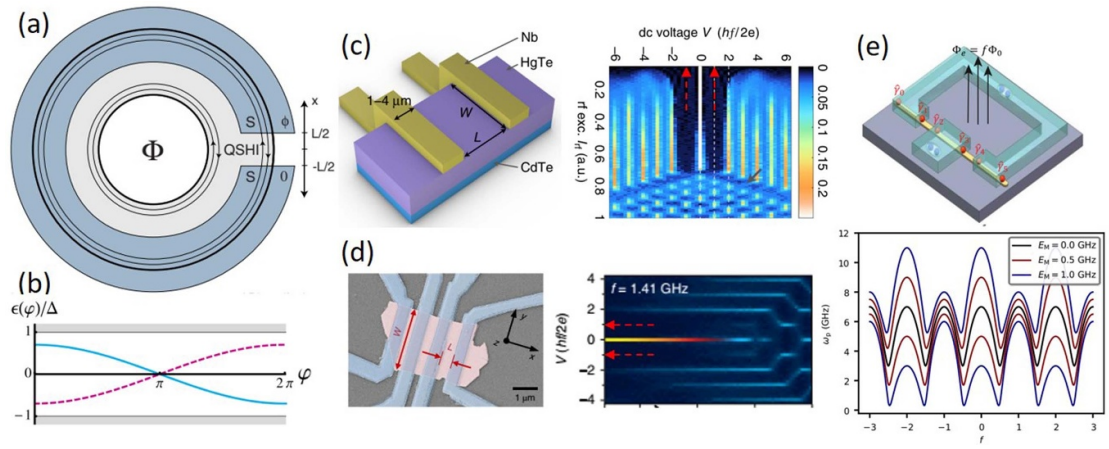

Figure 4. (a) A junction in an rf SQUID geometry where the edge states of quantum-spin-Hall insulator (QSHI) are coupled to a superconductor shaped as a Corbino disk. Reprinted figure with permission from [48], Copyright (2009) by the American Physical Society. (b) Spectrum of Andreev bound states in the topological junction shown in (a) as a function of phase difference φ. Reprinted from [49], Copyright (2013), with permission from Elsevier. (c) A topological JJ composed of 2D TI (HgTe) and its Shapiro step measurements (the missing $n = 1$ steps are indicated by the red arrows in the right panel). Reproduced from [15]. CC BY 4.0. (d) A topological JJ composed of Dirac semimetal ($Bi_{0.97}Sb_{0.03}$) and its Shapiro step measurements (the missing $n = 1$ steps are indicated by the red arrows in the right panel). Reproduced from [18], with permission from Springer Nature. (e) Schematic of a split transmon qubit hosting MZMs (top panel), and its excitation spectrum as a function of magnetic flux f (Φ_e/Φ_0) (bottom panel). Reproduced from [52]. CC BY 4.0.

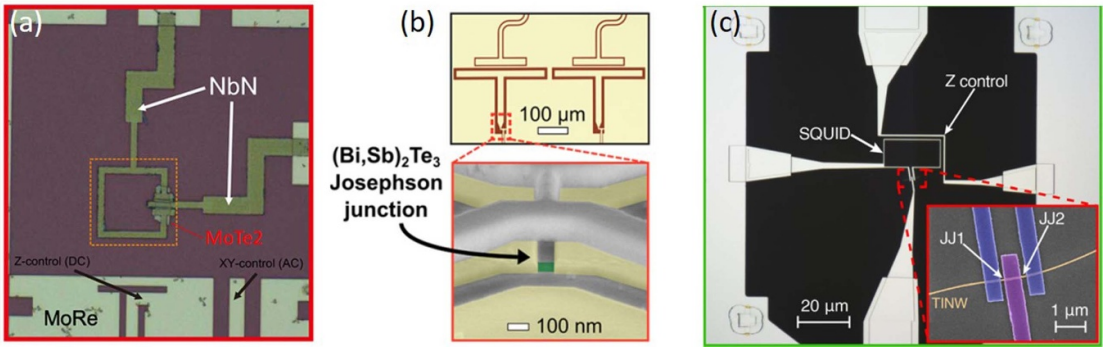

Figure 5. (a) Superconducting quantum circuit based on Weyl semimetal $MoTe_2$. Reprinted with permission from [51]. Copyright (2020) American Chemical Society. (b) Topological insulator (TI) $(Bi_{0.06}Sb_{0.94})_2Te_3$ transmon. Reprinted with permission from [28]. Copyright (2022) American Chemical Society. (c) A flux-tunable TI (Bi_2Se_3) nanowire transmon. Inset shows the false-color SEM image of the nanowire SQUID. Reprinted from [30], with the permission of AIP Publishing.

$(Bi,Sb)_2Te_3$ TI nanoribbon weak links [28]. In this device, coherent qubit control, including Rabi oscillations and Ramsey interference patterns, was demonstrated, with reported values of $T_1 \approx 28$ ns and $T_2^* \approx 10$ ns [28]. The authors of this study suggest that the quality of the JJ, rather than the TLS losses in the bulk, is responsible for the short coherence time [28]. Figure 5(c) shows a flux-tunable transmon consisting of a Bi_2Se_3 TI nanowire SQUID [30]. Rabi oscillations and a relatively long $T_1 \approx 0.5$ μs were observed; however, the estimated dephasing time T_2, obtained by fitting the spectral line, is short, ranging from approximately 1 to 4 ns. In addition, T_2 is reported to depend on $\partial f_{01}/\partial\Phi$. Therefore, the reason for the particular short T_2 was attributed to the qubit frequency fluctuations caused by low-frequency flux noise, which could be reduced by using on-chip flux traps, better twisted bias wires and low-pass filters in the future [30].

2.5. Integration with 3D cavities

Most previously introduced QM-based c-QED devices were coupled with 2D coplanar readout resonators. In contrast, 3D transmons and their integration with 3D cavities as readout resonators offer several advantages over their 2D counterparts. 3D cavities offer a simpler electromagnetic environment for superconducting qubits, reducing dielectric loss and enhancing performance [54]. They also allow easy tuning of c-QED parameters, such as cavity decay rate (κ) and qubit–cavity coupling strength (g), by adjusting the readout pin length and qubit position—an advantage not possible with fixed 2D resonators [55]. Additionally, their straightforward design and fabrication accelerate measurement cycles. Integration of QMs into 3D cavities

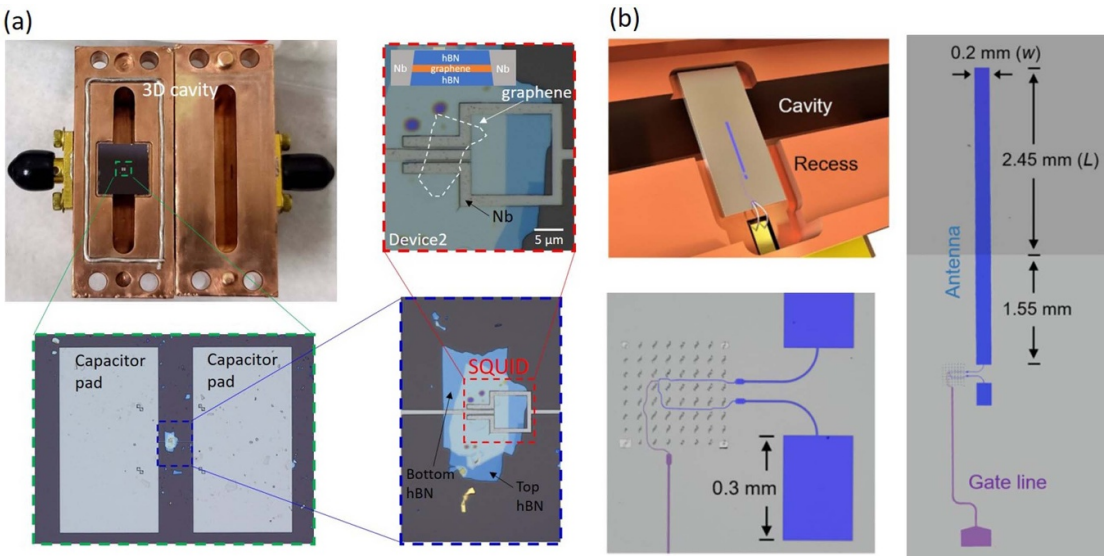

Figure 6. (a) A flux tunable graphene-based superconducting quantum circuit coupled to 3D cavity. Reprinted figure with permission from [53], Copyright (2025) by the American Physical Society. (b) An InAs nanowire gatemon realized in 3D cavity. Reprinted figure with permission from [31], Copyright (2024) by the American Physical Society.

was first realized in MoS_2 vertical JJs [43], then extended to graphene SQUIDs (figure 6(a)) and InAs nanowire JJs (figure 6(b)), respectively [31, 53]. The graphene SQUID device shown in figure 6(a) consists of a pair of capacitor pads, which serve as the antenna to interact with microwave in a 3D cavity as well as for the bond pads in DC transport measurements. The correlations between DC and RF measurements-including the Fraunhofer pattern, flux-modulated supercurrent, and the corresponding resonator frequency-were studied across three devices with varying degrees of SQUID symmetry. However, coherent control of qubits was not reported in this paper [53]. Figure 6(b) presents a 3D gatemon using InAs nanowire as a weak link and a copper cavity as readout resonators [31]. In this study, the gate line is located away from the chamber of 3D cavity, which greatly preserve the quality factor of the readout cavity. The gate-tunable resonator frequency (one-tone measurements) and qubit transition spectroscopy (two-tone measurements) are demonstrated, as well as Rabi oscillations with a Rabi coherence time $T_R \approx 260 \pm 60$ ns. However, further time-domain measurements for $T1$ and T_2^* are unsuccessful due to device instabilities [31]. The two studies have potential applications in probing MZMs, which we will further discuss in the outlook section.

2.6. Other components in c-QED devices

Apart from the Josephson weak links, QMs have also been investigated for uses in different components of superconducting qubits. Conventional transmons utilize capacitors with a large footprint ($\approx 10^5\ \mu m^2$) to acquire sufficient capacitance. These capacitors consist of large planar electrodes without dielectric materials, minimizing TLS-induced decoherence and preserving qubit coherence, but at the expense of significant space and cross-talk between neighboring qubits [35, 56]. Therefore, it is desirable to have a lumped-element device with a high-quality dielectric to contain electric field in a small region with low loss, forming qubits with reduced size and low cross-talk [36]. Such a concept was explored by using vdW PPCs consisting of superconducting $NbSe_2$ and insulating hBN [35, 36]. Those capacitors were integrated with conventional Al/Al_2O_3-based JJs to form transmons (figure 7(a)), with a 1400 times smaller capacitor size while maintaining a qubit coherence time around 1–2 μs [35]. The coherence time of conventional transmons with large capacitor pads fabricated on the same substrate is reported as $T_1 \approx 11.5\ \mu s$ and $T_2^* \approx 10.5\ \mu s$. This suggests that JJs are not the limiting factor for qubit coherence. Instead, qubit coupling to residual elements outside the PPC, introduced during the vdW stacking process or Al lift-off, may contribute to the reduced coherence time [35]. In another work with similar designs (figure 7(b)), the coherence time of the PPC-based qubits was further extended to 25 μs, while conventional Xmons fabricated on the same substrate exhibited coherence times ranging from 38 to 49 μs [36]. It is believed that optimizing the fabrication process and confining the electric field within the pristine interior of the vdW PPC could further extend the coherence time [35].

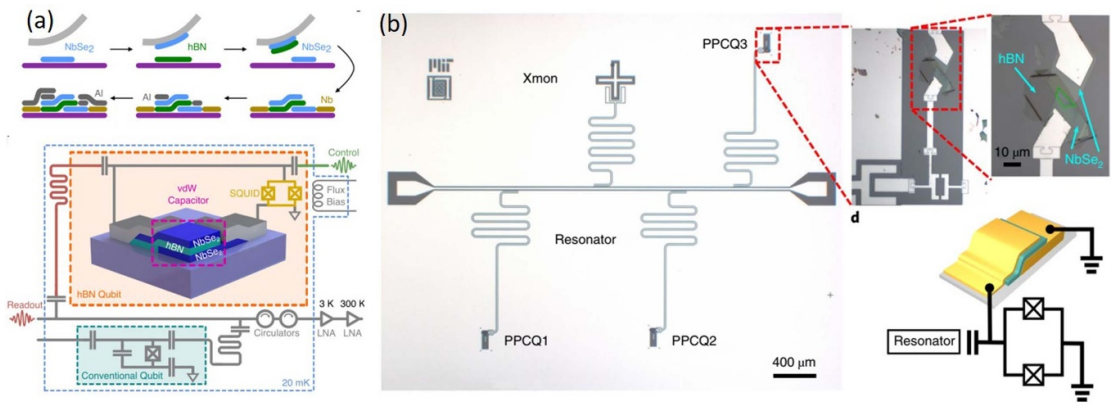

Figure 7. (a) Capacitor consists of $NbSe_2$ and hBN, which is integrated with a Al/Al_2O_3-based SQUID to form a transmon. Reprinted with permission from [35]. Copyright (2021) American Chemical Society. (b) Another work with similar design of (a), showing improved qubit coherence time. Reproduced from [36], with permission from Springer Nature.

3. Outlook

Early studies of gatemons have not reported a strong correlation between coherence time and gate voltage, making it difficult to determine the impact of charge noise induced by the gate electrode on qubit coherence [21, 22, 25, 26]. The main limiting factor of coherence time was attributed to capacitive coupling between the qubit shunting capacitor and the backgate for graphene gatemons [21], and to dielectric loss in the qubit capacitor for 2DEG gatemons [22]. In contrast, the InAs nanowire gatemons in [29] exhibit a strong correlation between coherence time and gate voltage, and the authors conclude that, in such devices, on-chip charge noise dominates over electrical noise on the gate [29]. It is worth noting that in these QM-based transmons, the transfer of QMs is generally required [57, 58], which may inevitably leave polymer residues or QM residues on the substrate. These residues can be major source for on-chip dielectric loss [53]. Therefore, careful surface cleaning, as well as maintaining cleanliness at the S–N–S junction interfaces, is expected to play a crucial role in improving coherence time. In addition, drawing inspiration from the improved coherence time in superconducting qubits achieved by replacing the substrate with sapphire [41] and incorporating tantalum as a resonator [59], these approaches should be considered as future directions for further enhancing the coherence of QM-based transmons.

The QM-based fluxonium is an intriguing platform to explore, although good coherence properties have not yet been reported so far [33, 34]. The current InAs 2DEG gatemoniums exhibit a shorter coherence time ($T_1 \approx 78$ ns and $T_2 \approx 102$ ns) [34] compared to InAs 2DEG gatemons ($T_1 \approx 0.8\,\mu$s and $T_2 \approx 1\,\mu$s) [22]. The short coherence times reported for the gatemoniums have primarily been attributed to inductive loss, which could be mitigated by increasing the thickness of the aluminum used for the electrodes in both the JJ and JJ array [34]. It would be interesting to observe whether these modifications allow the coherence time to approach the values reported for InAs 2DEG gatemons [22]. Furthermore, to better understand the effects of charge noise and flux noise on coherence properties, it would be valuable to investigate the correlation between coherence times and gate voltage or flux bias, as demonstrated in InAs nanowire transmons [29]. In addition, using high-kinetic-inductance materials to replace JJ array [34, 60], hence reducing the size of the superinductor, would also be an interesting direction to explore.

Vertical stacking architectures, including the METs with semiconductor tunnel barriers [44] and the PPCs with insulating dielectric hBN [35, 36], offer the potential to engineer superconducting qubits with significantly reduced capacitor sizes. However, no coherence properties have been reported for METs [44]. Further experimental studies are required to better understand the limiting factors, similar to the investigations conducted during the early development of QM-based gatemons [21, 22, 25, 26, 29]. Both QM-based METs and PPCs also need to consider mass production to enable qubit scaling. Therefore, studies on incorporating CVD-grown QMs into these elements and evaluating their performance are desirable.

For TI-based transmons, while their coherence times are short ($T_1 \approx 28$ ns and $T_2^* \approx 10$ ns for TI nanoribbons while $T_1 \approx 0.5\,\mu$s and $T_2 \approx 1$–4 ns for TI nanowires) [28, 30], they offer an interesting platform for probing MZMs. In topological SQUID-based transmons, the qubit frequency inherits the unconventional 4π-periodic supercurrent from the constituent topological JJs and exhibits a 4π-periodic modulation in response to the applied flux (see figure 4(e)) [49, 52]. Such a phenomenon has not been observed in $MoTe_2$ and Bi_2Se_3 nanowire SQUID-based transmons [30, 51]. However, one may need to consider quasiparticle

poisoning, which tend to restore the unconventional 4π periodicity to trivial 2π periodicity [49, 52]. Since the measurements conducted in [51] have an integration time around seconds, they may still suffer from the quasiparticle poisoning happening at a time scale around microseconds [51, 61]. Future experiments will require time-domain spectroscopy that operates faster than the quasiparticle poisoning timescale [52] to probe the 4π-periodic qubit frequency modulation. Furthermore, although beyond the scope of this paper, numerous proposals in the field of topological quantum computing suggest employing cQED techniques to probe and manipulate MZMs, and to realize topological qubits in hybrid devices [62–67].

The integration of 3D cavities is expected to provide a superior electromagnetic environment for superconducting qubits over their 2D counterparts [54]. However, no obvious improvement in coherence time has yet been observed in QM-based 3D devices to support this expectation [31, 43, 53]. This may suggest that the coherence properties reported to date are still primarily limited by the QM-based junctions themselves, thereby obscuring the potential advantages of the 3D cavity architecture. Further investigations into enhancing the quality of QM-based JJs and understanding their influence on the coherence of 3D transmons are desirable. It is also worth noting that, unlike conventional Al-based transmons, the QM-based transmons undergo different fabrication processes and often have QM and polymer residues that could introduce additional dielectric losses [53]. It may require a systematic study, comparing the same weak link materials with similar fabrication processes in both 2D and 3D transmon architectures, to better understand the benefits that 3D cavities can provide. Nevertheless, QM-based 3D transmons may still offer other advantages, such as enabling the exploration of MZM-related physics. The proximitized semiconductor nanowire in 3D copper cavities enables the application of a magnetic field to access the MZMs, without concerning the degradation of resonators in the 2D cases [31]. The platform described in [53], which enables both DC and RF measurements, is also advantageous for probing the 4π-periodic supercurrent associated with topological JJs. A valid topological JJ can first be identified by observing the absence of the $n = 1$ Shapiro step in DC transport [15, 16, 18]. The same device can then be placed in a 3D cavity to investigate the 4π modulation of the qubit frequency using time-domain spectroscopy, with the potential to mitigate quasiparticle poisoning [52]. This differs from resonator-type devices with embedded JJs [68] and inductively coupled RF-SQUIDs [69]. The former allows for DC measurements but does not function as a two-level system capable of qubit operations, while the latter enables the study of ABS dynamics using time-domain techniques but does not support DC measurements.

Finally, there are some possible directions unexplored, such as the integration of ferromagnetic materials into superconducting qubits [70, 71]. In a JJ where the superconducting electrodes (S) are separated by a ferromagnetic (F) material, a π-phase shift is introduced in the ground-state superconducting order parameter of the S–F–S junction, forming what is known as a π-junction [72, 73]. When such π-junction is integrated into a superconducting qubit based on a conventional SQUID architecture, it acts as a passive phase shifter and eliminates the need for an external flux bias to achieve optimal operation [74, 75]. This type of qubit is sometimes referred to as a 'quiet qubit', because it is expected to be efficiently decoupled from environmental noise [76, 77]. In a recent study, Kim *et al* realized a π-qubit operating optimally at zero flux bias by incorporating a ferromagnetic metal-based (PdNi) π-junction into an NbN/AlN/NbN-based superconducting flux qubit [71]. The measured lifetime of the π-qubit ($T_1 = 1.45\,\mu$s) was three orders of magnitude longer than that of a previously reported superconducting phase qubit coupled to a π-junction [70], but an order of magnitude shorter than that of a conventional flux qubit [71]. This suggests that, unlike in the previous case [70], the coherence time is not limited by other dominant loss mechanisms, but rather by the π-junction itself—specifically, by dissipation due to quasiparticles within the junction [71]. It has been proposed that using an underdamped π-junction—such as one based on an insulating tunnel barrier—offers a more promising route to achieving significantly longer coherence times [78]. Therefore, it is worth exploring the coherence properties of π-junction qubits composed of ferromagnetic insulators [79, 80], as opposed to ferromagnetic metals, as used in [71].

As a concluding remark, superconducting quantum circuits based on QMs offer the possibility of designing new types of quantum devices that are not only practically viable for quantum computing but also serve as platforms for exploring the underlying physics of their constituent materials. The fast microwave technology inherited from superconducting qubits provides a powerful tool for probing the fundamental properties of QMs, while the versatile functionalities of QMs contribute to the design of novel quantum devices. Therefore, research in this field holds significant potential for advancing both superconducting quantum computing and materials science.

Data availability statement

All data that support the findings of this study are included within the article (and any supplementary files).

Acknowledgments

Kuei-Lin Chiu would like to thank the funding supports from National Science and Technology Council (Grant No. NSTC 112-2112-M-110-017 and NSTC 113-2112-M-110-015) and Higher Education Sprout Project by the Ministry of Education (MOE) in Taiwan.

ORCID iDs

Avishma J Lasrado https://orcid.org/0009-0005-8912-0045
Cheng-Han Lo https://orcid.org/0009-0007-5798-1208
Chung-Ting Ke https://orcid.org/0000-0002-6031-4226

References

[1] Chiu K-L and Xu Y 2017 *Phys. Rep.* **669** 1
[2] Chiu K L 2020 *21st Century Nanoscience–A Handbook: Nanophotonics, Nanoelectronics and Nanoplasmonics* (CRC Press) pp 13–1–13–48
[3] Liu X and Hersam M C 2019 *Nat. Rev. Mater.* **4** 669
[4] Siddiqi I 2021 *Nat. Rev. Mater.* **6** 875
[5] Alfieri A, Anantharaman S B, Zhang H and Jariwala D 2024 *Adv. Mater.* **35** 2109621
[6] Qian X, Liu J, Fu L and Li J 2014 *Science* **346** 1344
[7] Wu S, Fatemi V, Gibson Q D, Watanabe K, Taniguchi T, Cava R J and Jarillo-Herrero P 2018 *Science* **359** 76
[8] Cao Y, Fatemi V, Fang S, Watanabe K, Taniguchi T, Kaxiras E and Jarillo-Herrero P 2018 *Nature* **556** 43
[9] Xia Y, Han Z, Watanabe K, Taniguchi T, Shan J and Mak K F 2024 arXiv:2405.14784
[10] Krantz P, Kjaergaard M, Yan F, Orlando T P, Gustavsson S and Oliver W D 2020 *Appl. Phys. Rev.* **6** 021318
[11] Blais A, Grimsmo A L, Girvin S M and Wallraff A 2021 *Rev. Mod. Phys.* **93** 025005
[12] Mourik V, Zuo K, Frolov S M, Plissard S R, Bakkers E P A M and Kouwenhoven L P 2012 *Science* **336** 1003
[13] Albrecht S M, Higginbotham A P, Madsen M, Kuemmeth F, Jespersen T S, Nygrd J, Krogstrup P and Marcus C M 2016 *Nature* **531** 206
[14] Fu J-B, Li B, Zhang X-F, Yu G-Z, Huang G-Y and Deng M-T 2021 *Science China Physics, Mechanics & Astronomy* **64** 107001
[15] Wiedenmann J *et al* 2016 *Nat. Commun.* **7** 10303
[16] Bocquillon E, Deacon R S, Wiedenmann J, Leubner P, Klapwijk T M, Brüne C, Ishibashi K, Buhmann H and Molenkamp L W 2017 *Nat. Nanotechnol.* **12** 137
[17] Wang A-Q, Li C-Z, Li C, Liao Z-M, Brinkman A and Yu D-P 2018 *Phys. Rev. Lett.* **121** 237701
[18] Li C, de Boer J C, de Ronde B, Ramankutty S V, van Heumen E, Huang Y, de Visser A, Golubov A A, Golden M S and Brinkman A 2018 *Nat. Mater.* **17** 875
[19] Randle M D *et al* 2024 *Adv. Mater.* **35** 2301683
[20] Kroll J G, Uilhoorn W, van der Enden K L, de Jong D, Watanabe K, Taniguchi T, Goswami S, Cassidy M C and Kouwenhoven L P 2018 *Nat. Commun.* **9** 4615
[21] Wang J I-J *et al* 2019 *Nat. Nanotechnol.* **14** 120
[22] Casparis L *et al* 2018 *Nat. Nanotechnol.* **13** 915–9
[23] Hertel A *et al* 2022 *Phys. Rev. Appl.* **18** 034042
[24] Lo C-H, Chen Y-H, Lasrado A J, Kuo T, Chang Y-Y, Hsu T-Y, Chen Y-C, Guo G-P and Chiu K-L 2023 *SPIN* **13** 2340021
[25] Larsen T W, Petersson K D, Kuemmeth F, Jespersen T S, Krogstrup P, J Nygård and Marcus C M 2015 *Phys. Rev. Lett.* **115** 127001
[26] de Lange G, van Heck B, Bruno A, van Woerkom D J, Geresdi A, Plissard S R, Bakkers E P A M, Akhmerov A R and DiCarlo L 2015 *Phys. Rev. Lett.* **115** 127002
[27] Huo J *et al* 2023 *Chin. Phys. Lett.* **40** 047302
[28] Schmitt T W *et al* 2022 *Nano Lett.* **22** 2595
[29] Luthi F *et al* 2018 *Phys. Rev. Lett.* **120** 100502
[30] Sun X *et al* 2023 *Appl. Phys. Lett.* **122** 154001
[31] Xia Z *et al* 2024 *Phys. Rev. Appl.* **21** 034031
[32] Strickland W M *et al* 2024 *Phys. Rev. Res.* **6** 023094
[33] Pita-Vidal M, Bargerbos A, Yang C-K, van Woerkom D J, Pfaff W, Haider N, Krogstrup P, Kouwenhoven L P, de Lange G and Kou A 2020 *Phys. Rev. Appl.* **14** 064038
[34] Strickland W M, Elfeky B H, Baker L, Maiani A, Lee J, Levy I, Issokson J, Vrajitoarea A and Shabani J 2025 *PRX Quantum* **6** 010326
[35] Antony A *et al* 2021 *Nano Lett.* **21** 10122
[36] Wang J I-J *et al* 2022 *Nat. Mater.* **21** 398
[37] Wang I-J 2016 *Doctoral Dissertation* Harvard University (available at: https://dash.harvard.edu/handle/1/26718763)
[38] Larsen T W, Gershenson M E, Casparis L, Kringhøj A, Pearson N J, McNeil R P G, Kuemmeth F, Krogstrup P, Petersson K D and Marcus C M 2020 *Phys. Rev. Lett.* **125** 056801
[39] Manucharyan V E, Koch J, Glazman L I and Devoret M H 2009 *Science* **326** 113
[40] Earnest N *et al* 2018 *Phys. Rev. Lett.* **120** 150504
[41] Somoroff A, Ficheux Q, Mencia R A, Xiong H, Kuzmin R and Manucharyan V E 2023 *Phys. Rev. Lett.* **130** 267001
[42] Wang F *et al* 2024 Achieving millisecond coherence fluxonium through overlap josephson junctions (arXiv:2405.05481)
[43] Lee K-H *et al* 2019 *Nano Lett.* **19** 8287
[44] Balgley J *et al* 2025 arXiv:2501.14969
[45] Willsch D *et al* 2024 *Nat. Phys.* **20** 815
[46] Zhao R, Park S, Zhao T, Bal M, McRae C R H, Long J and Pappas D P 2020 *Phys. Rev. Appl.* **14** 064006
[47] Nayak C, Simon S H, Stern A, Freedman M and Das Sarma S 2008 *Rev. Mod. Phys.* **80** 1083
[48] Fu L and Kane C L 2009 *Phys. Rev. B* **79** 161408

[49] Badiane D M, Glazman L I, Houzet M and Meyer J S 2013 *C. R. Physique* **14** 840
[50] Shvetsov O O, Kononov A, Timonina A V, Kolesnikov N N and Deviatov E V 2018 arXiv:1801.09551
[51] Chiu K-L, Qian D, Qiu J, Liu W, Tan D, Mosallanejad V, Liu S, Zhang Z, Zhao Y and Yu D 2020 *Nano Lett.* **20** 8469
[52] Sun X *et al* 2022 arXiv:2211.08094
[53] Chiu K-L *et al* 2025 *Phys. Rev. Appl.* **23** 034059
[54] Paik H *et al* 2011 *Phys. Rev. Lett.* **107** 240501
[55] Zoepfl D, Muppalla P R, Schneider C M F, Kasemann S, Partel S and Kirchmair G 2017 *AIP Adv.* **7** 085118
[56] Kjaergaard M *et al* 2022 *Phys. Rev. X* **12** 011005
[57] Dean C R *et al* 2010 *Nat. Nano* **5** 722
[58] Wang L *et al* 2013 *Science* **342** 614
[59] Bal M *et al* 2024 *npj Quantum Inf.* **10** 43
[60] Tanaka M *et al* 2025 *Nature* **638** 99
[61] Rainis D and Loss D 2012 *Phys. Rev. B* **85** 174533
[62] Hassler F, Akhmerov A R and Beenakker C W J 2011 *New J. Phys.* **13** 095004
[63] Hyart T, van Heck B, Fulga I C, Burrello M, Akhmerov A R and Beenakker C W J 2013 *Phys. Rev. B* **88** 035121
[64] Pekker D, Hou C-Y, Manucharyan V E and Demler E 2013 *Phys. Rev. Lett.* **111** 107007
[65] Ginossar E and Grosfeld E 2014 *Nat. Commun.* **5** 4772
[66] Yavilberg K, Ginossar E and Grosfeld E 2019 *Phys. Rev. B* **100** 241408
[67] Ávila J, Prada E, San-Jose P and Aguado R 2020 *Phys. Rev. Res.* **2** 033493
[68] Schmidt F E, Jenkins M D, Watanabe K, Taniguchi T and Steele G A 2018 *Nat. Commun.* **9** 4069
[69] Hays M, de Lange G, Serniak K, van Woerkom D J, Bouman D, Krogstrup P, Nygård J, Geresdi A and Devoret M H 2018 *Phys. Rev. Lett.* **121** 047001
[70] Feofanov A K *et al* 2010 *Nat. Phys.* **6** 593
[71] Kim S, Abdurakhimov L V, Pham D, Qiu W, Terai H, Ashhab S, Saito S, Yamashita T and Semba K 2024 *Commun. Mater.* **5** 216
[72] Buzdin A, Bulaevskii L and Panyukov S 1982 *JETP Lett.* **35** 178–80
[73] Ryazanov V V, Oboznov V A, Rusanov A Y, Veretennikov A V, Golubov A A and Aarts J 2001 *Phys. Rev. Lett.* **86** 2427
[74] Shcherbakova A V *et al* 2015 *Supercond. Sci. Technol.* **28** 025009
[75] Yamashita T, Kim S, Kato H, Qiu W, Semba K, Fujimaki A and Terai H 2020 *Sci. Rep.* **10** 13687
[76] Ioffe L B, Geshkenbein V B, Feigel'man M V, Fauchère A L and Blatter G 1999 *Nature* **398** 679
[77] Blatter G, Geshkenbein V B and Ioffe L B 2001 *Phys. Rev. B* **63** 174511
[78] Kato T, Golubov A A and Nakamura Y 2007 *Phys. Rev. B* **76** 172502
[79] Huang B *et al* 2017 *Nature* **546** 270
[80] Gong C *et al* 2017 *Nature* **546** 265